

Review

Microwave SINIS Detectors

Mikhail Tarasov ^{1,*} , Aleksandra Gunbina ² , Artem Chekushkin ¹, Renat Yusupov ¹ , Valerian Edelman ³
and Valery Koshelets ¹¹ V. Kotelnikov Institute of Radio Engineering and Electronics of RAS, 103907 Moscow, Russia² Institute of Applied Physics of RAS, 603155 Nizhny Novgorod, Russia³ P. Kapitza Institute for Physical Problems of RAS, 119334 Moscow, Russia

* Correspondence: tarasov@hitech.cplire.ru

Featured Application: Among cryogenic microwave detectors and bolometers, the SINIS detectors are promising candidates for practical applications due to their wide dynamic range, low requirements for temperature stabilization, lack of upper limit for signal frequency, and immunity to vibrations and magnetic fields compared to competing cryogenic detectors such as transition edge sensors, kinetic inductance detectors, hot electron detectors, and SIS detectors.

Abstract: This review presents the main characteristics and mechanisms of operation of superconductor–insulator–normal metal–insulator–superconductor (SINIS) microwave detectors. An analysis of the detectors' performance against a quantum detector and a photon counter is given. Methods for cooling a superconductor using normal metal traps and the role of electron cooling in optimizing the current response to terahertz radiation are discussed. Fabrication methods using shadow evaporation as well as magnetron sputtering are described.

Keywords: SINIS structures; superconductivity; thin-film technology; tunnel junctions; subTHz detectors; planar antenna arrays



Citation: Tarasov, M.; Gunbina, A.; Chekushkin, A.; Yusupov, R.; Edelman, V.; Koshelets, V. Microwave SINIS Detectors. *Appl. Sci.* **2022**, *12*, 10525. <https://doi.org/10.3390/app122010525>

Academic Editor: Ernesto Limiti

Received: 3 October 2022

Accepted: 17 October 2022

Published: 18 October 2022

Publisher's Note: MDPI stays neutral with regard to jurisdictional claims in published maps and institutional affiliations.



Copyright: © 2022 by the authors. Licensee MDPI, Basel, Switzerland. This article is an open access article distributed under the terms and conditions of the Creative Commons Attribution (CC BY) license (<https://creativecommons.org/licenses/by/4.0/>).

1. Introduction

Normal metal–insulator–superconductors (NISs), as well as SIS tunnel junctions, are the main building blocks in superconducting electronics. SINIS is one of the generic elements of a wide family of cryogenic devices [1–3], such as Andreev bolometers (AB) [4,5], normal metal hot-electron bolometers (NHEB) [6], cold-electron bolometers (CEB) [7,8], SINIS bolometers [9–11], SINIS detectors [12–14], NIS array thermometers [15–17], electron coolers [18–21], and photon counters. Over the 30 years in which they have been in development, detectors with NIS tunnel junctions have been referred to as ANHEB—a normal metal hot-electron bolometer with Andreev reflection (SNS + NIS), actually operating at frequencies below 70 GHz; CCNHEB [22]—capacitive coupled normal metal hot-electron bolometers (SINIS); CEB—cold-electron bolometers (SINIS), which are the same as CCNHEB, but operate with electron cooling; SINIS detectors—an SINIS structure in the operation mode of quantum response, at frequencies above 70 GHz; an NISIN detector with a structure similar to SINIS, or even NININ or MIMIM detectors with metal–insulator–metal tunnel junctions [23,24].

A hot-electron bolometer with Andreev contacts between the N-absorber and S-electrodes, and with an NIS thermometer for temperature response measurement, was proposed in a publication [5]—see the schematic view in Figure 1. Such a bolometer demonstrated, under dc heating, a responsivity of up to 10^9 V/W and a noise equivalent power (NEP) = 3×10^{-19} W/Hz^{1/2}.

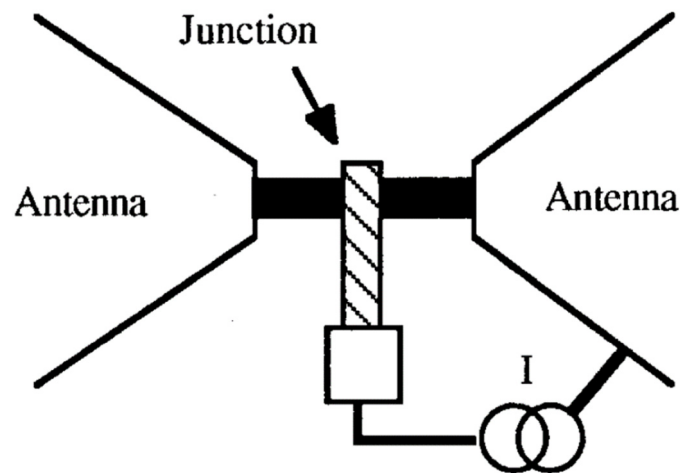


Figure 1. Basic schematics of ANHEB with superconducting antenna directly connected via Andreev junctions to normal metal absorber (black), and NIS junction thermometer connected to current source I.

One of the first attempts to study ANHEB bolometers (Figure 2) under microwaves was made in [4], in which, under dc heating, $NEP_{dc} = 5 \times 10^{-18} \text{ W/Hz}^{1/2}$ was obtained and at 300 GHz irradiation, only $NEP_{microwave} = 10^{-14} \text{ W/Hz}^{1/2}$ and $dV/dP = 10^6 \text{ V/W}$ were reached, whose values are much lower compared to the response at dc or low frequencies.

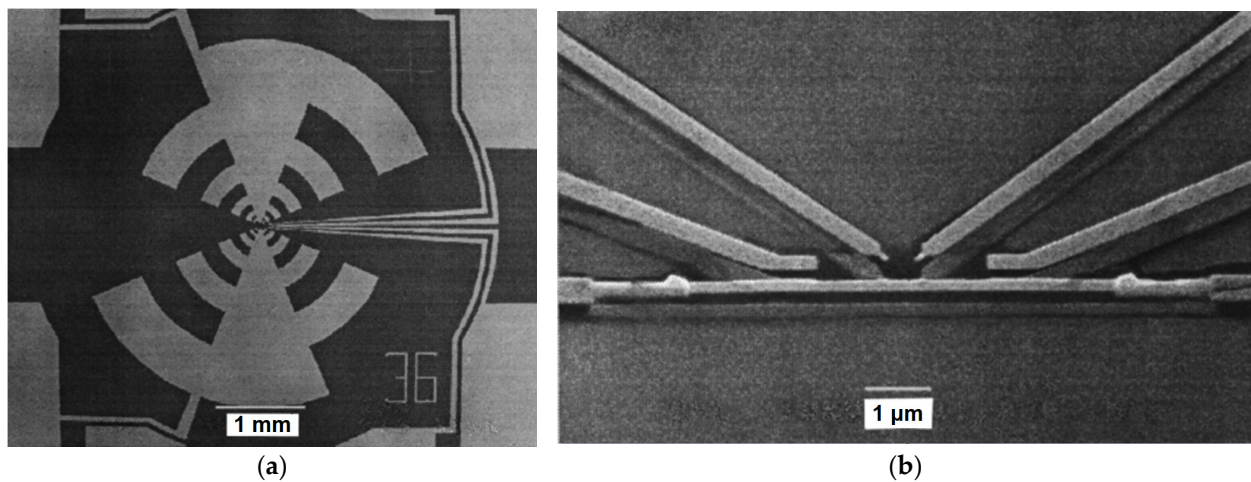


Figure 2. SEM view of ANHEB integrated in log-periodic mode (a) and a microbolometer (b) [4].

The reason for this contradiction is that Andreev contacts are transparent to electrons with energy above the superconducting aluminum gap, which is about 70 GHz. This became clear in 2001 after theoretical analyses performed by Devyatov. A solution to increasing the signal frequency was found by Likharev, who proposed replacing the Andreev contacts with tunnel NIS junctions. The first practical results of an SINIS microwave detector were obtained in 2001 at Chalmers University of Technology [22], and these are described in detail in [25].

In the same year, pioneering work on electron cooling using NIS junctions appeared [26,27]. As Devyatov noted, since the NIS junction provides electron cooling, such cooling can also occur in the bolometer, so under certain modes of operation of the SINIS structure, it can switch from a hot-electron bolometer (HEB) operation mode to a cold-electron bolometer (CEB) mode, as was first proposed in [28]. In such a bolometer, at a dc bias close to the energy gap, it is possible to obtain electron cooling from the phonon temperature of 300 mK

down to the electron temperature of about 100 mK, thus theoretically reducing the dc NEP to 10^{-18} W/Hz^{1/2}.

Depending on the frequency range and the required bandwidth, the designs of bolometers with different planar antennas were fabricated and experimentally studied. Such integrated antenna–SINIS structures were assessed in quasioptical lens systems, and optical response values up to 0.8×10^9 V/W and $\text{NEP} = 2 \times 10^{-17}$ W/Hz^{1/2} were obtained at frequencies around 350 GHz.

Besides SINIS structures, we also studied a close relative—NININ or MIMIM structures [23,24], which are transformed from SINISs at bath temperatures above the critical temperature of the superconductor. Surprisingly, such a simple structure can also operate as a microwave detector with moderate sensitivity.

2. Electron Cooling

The effect of electron cooling ostensibly seems very promising; however, its effects are twofold. In actuality, electron cooling leads to a decrease in the current response and an increase in the shot noise. As a result, it does not contribute much to the improvement of the NEP. Since the noise emerging from the electron–phonon heat flow is $\text{NEP}_{\text{e-ph}}^2 = 10k\nu\Sigma(T_e^6 + T_{\text{ph}}^6)$, in which k is the Boltzman constant, ν is the absorber volume, and Σ is the material constant [29], the total $\text{NEP}_{\text{e-ph}}$ is mainly determined by the highest temperature, and only cooling the electron component does not improve the performance of the device much compared to cooling both components. If we take $T_e = 0.1$ K and $T_p = 0.3$ K for electron cooling only, and compare the results to $T_e = T_p = 0.1$ K for the cooling of both, the difference between $\text{NEP}_{0.3}$ and $\text{NEP}_{0.1}$ is 20 times. Besides this, a shot noise component derived from electron cooling heat flow P_{cool} will add $\text{NEP}^2 = 4kT_0P_{\text{cool}}$ and additional shot noise due to the higher dc current bias, $\text{NEP}_{\text{SIN}}^2 = 2eI_{\text{dc}}/(dI/dP)^2$. This is accompanied by the problem of the heat sink from the superconducting electrodes in the high-dc bias mode required for electron cooling, which can lead to an increase in both the superconductor electron temperature and the phonon temperature of the chip.

As mentioned in [30], and shown in Figure 3, at voltages below the superconducting gap, the electron temperature T_e at the substrate temperature $T \sim 0.1$ K is ~ 0.23 K due to overheating caused by spurious radiation. At the substrate temperature $T \sim 0.3$ K, the electron temperature is close to the substrate temperature $T_e \approx T$. In both cases, with an increase in bias voltage, T_e decreases due to electron cooling and reaches 0.19 K at a voltage corresponding to the maximum response. The response at $T = 0.1$ K is greater than that at $T \sim 0.3$ K by a factor of 5–6. Thus, the cooling of electrons alone does not provide the same responsivity as the cooling of the detector as a whole.

Thus, our direct experiment does not support our hypothesis that without decreasing the phonon temperature of the SINIS detector, it is possible to achieve optimal responsivity. Such cooling requires dilution cryostats or adiabatic demagnetization refrigerators (ADR); using ³He sorption cryostats is not enough, and electron cooling does not help.

On the other hand, if we fabricate a suspended N absorber in the SINIS structure, it is much easier to achieve both electron cooling and phonon cooling in the long N absorber, especially when the material of the absorber is different from that of the superconducting electrodes, such as for a Pd and Al pair. In this case, the acoustic mismatch provides moderate thermal insulation for phonon temperature, and substantial phonon cooling can be achieved.

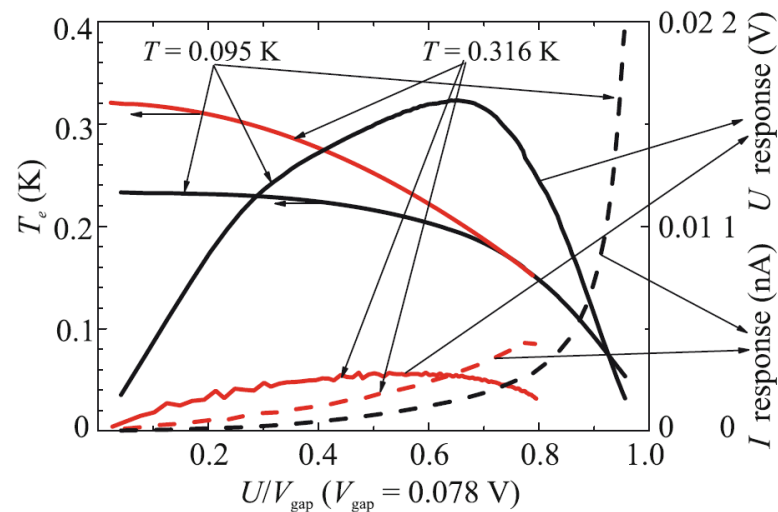


Figure 3. Voltage dependences of the electron temperature of the normal absorber of the detector (left scale) and of the voltage and current responses (right scale) at temperatures of $(0.095 \pm 0.01) \text{ K}$ and $(0.316 \pm 0.02) \text{ K}$ when irradiated with a black body radiation source. Red lines show the results for the temperature of the sample holder $T = 0.32 \text{ K}$, with black lines for the temperature $T = 0.1 \text{ K}$. Solid lines belonging to the right scale show voltage responses, while dotted lines show current responses. Graph from [30].

3. Quantum and Bolometric Response

The key issue when estimating the efficiency and performance margins of such a detector is the response origin or mechanism of detection. Earlier publications [7] adopted the bolometric approach, which predicts high responsivity at dc or a low frequency signal below 70 GHz for aluminum SINIS. The development of quantum response theory [12] has made it possible to adequately describe processes at higher frequencies. A detailed experimental study of the transition from thermal absorption to quantum efficiency was carried out in [31] (schematic image of SINIS detector—see Figure 4). It was experimentally demonstrated that the thermal contact of the absorber and substrate could significantly reduce the responsivity.

The important conclusion drawn in [12,31] is that electron cooling does not lead to an increase in sensitivity. We analyzed the characteristic time constants of energy relaxation in different SINIS structures. The most advantageous was the device with a suspended absorber, without losses of heat to the substrate [14].

The full description of the process of THz photon absorption in SINIS structures is rather complicated; it is not limited to a simple single electron–phonon interaction. For photons with energy significantly above the thermal energy, the energy of the electron that absorbs such a photon should correspond to the high electron temperature of about $hf = kT_e$, that is, 15 K for 350 GHz. The electron–electron interaction time at this temperature is much longer compared to the electron–phonon interaction time. As a result, a high-energy phonon is created. This phonon has three ways to escape: in the substrate, in the superconducting electrodes, or in the electron system with a quantum efficiency of 0.023 electrons per quantum at 1 THz. This is accompanied by the creation of an electron and hole pair, each of which have an energy of $hf/2$. An excited electron with energy $hf/2$ will create a phonon with the same energy of $hf/2$, corresponding to an electron temperature of 7 K, which again will create an electron–hole pair with energies $hf/4$; for this couple, the electron–electron interaction will be more efficient, and this leads to the creation of two excited electrons and one hole, with energy values of $hf/12$ each. At this step, the electron–electron interaction dominates, and leads to the effective multiplication of remaining excitations.

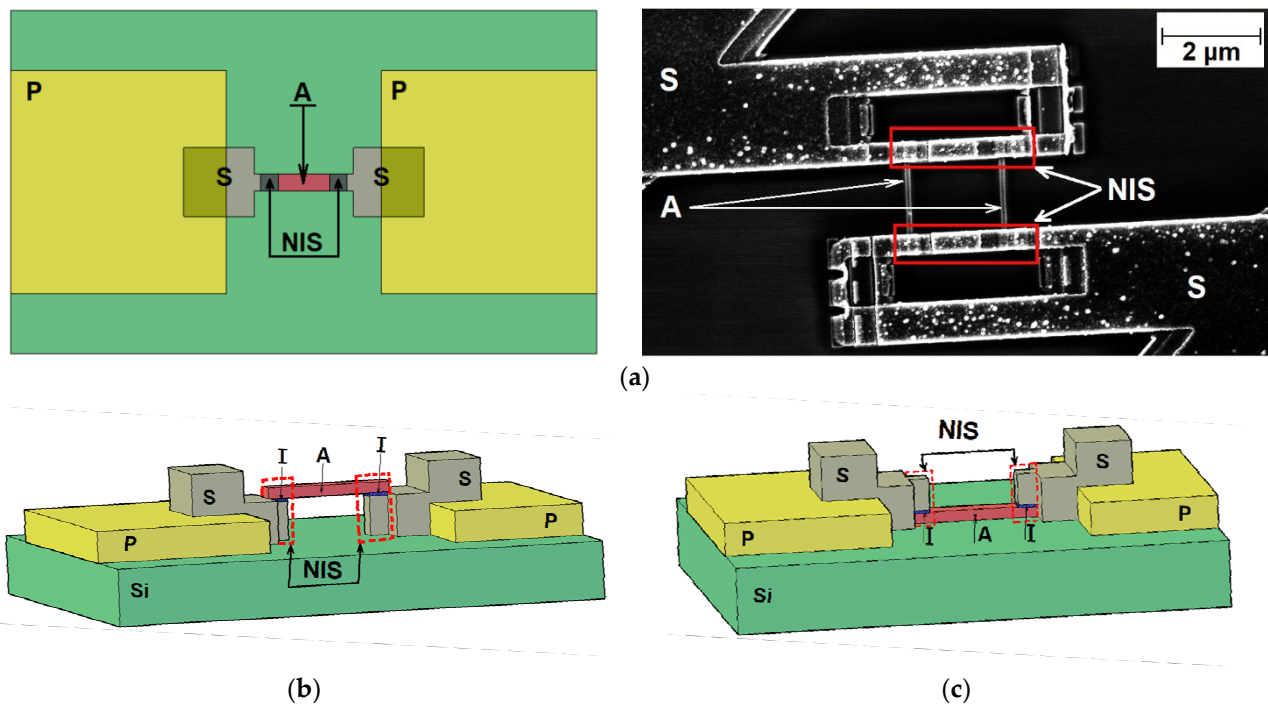


Figure 4. SINIS detector: (a) top view, schematic image (left) and SEM photo (right); (b) schematic image of SINIS detector with suspended absorber; (c) schematic image of SINIS detector with absorber on substrate. S—superconductor, I—insulator, A—absorber (normal metal), P—pads (supply electrodes).

Estimations of responsivity, in this case, are based on nonequilibrium electron and phonon distribution functions and mechanisms of quantum absorption [12]. The important figure is the quantum efficiency, which is equal to the number of excited and detected electrons for one absorbed photon. It can approach the value of $n = hf/kT$. However, if the dc bias is close to the energy gap, electron cooling effectively removes excited electrons from the absorber. Excited electrons cannot be multiplied, and the quantum efficiency drops to $n = 1$. According to this model, we can distinguish two operation modes: photon counter and quantum detector–multiplier modes. The current responsivity in the first case is $dq/dE = e/hf$, and it is e/kT in the second case. With an increase in frequency, the current responsivity of the photon counter drops, and when using a bolometer detector, the multiplier remains high—see Figure 5. The blue curve corresponds to the bolometric mode at a bias close to the gap voltage, with $dI/dP = e/2kT = 2.2 \times 10^4$ A/W; the dashed blue line is the half-gap bias, and $dI/dP = e/0.5\Delta = 5 \times 10^4$ A/W; the red curve represents the photon counter mode, with $dI/dP = e/hf = 762$ A/W at 350 GHz.

In Table 1, we also present the estimated voltage and current responsivity for a signal frequency of 350 GHz and a bath temperature of 280 mK. The maximum voltage responsivity is calculated at the half-gap voltage bias and a dynamic resistance of 35 k Ω for an SINIS detector with a normal resistance of 1 k Ω . The moderate multiplication of hot electrons occurs at about half gap.

Detection with high quantum efficiency can be obtained using the SINIS structure with a suspended normal metal absorber made of heavy metal. In SINIS, the Kapitza resistance between Al and Pd is high, and the electron–phonon interaction is low. For comparison, it is also important to mention that optimal resistance for quantum multiplication is 5 k Ω , contrary to the case of electron cooling, wherein the optimal resistance is about 0.5 k Ω .

Our measurements of SINIS detectors with suspended absorbers made of Cu, Hf, and Pd confirm the model of quantum absorption at 350 GHz with a quantum efficiency reaching 15 electrons for one photon [14] (Figure 6).

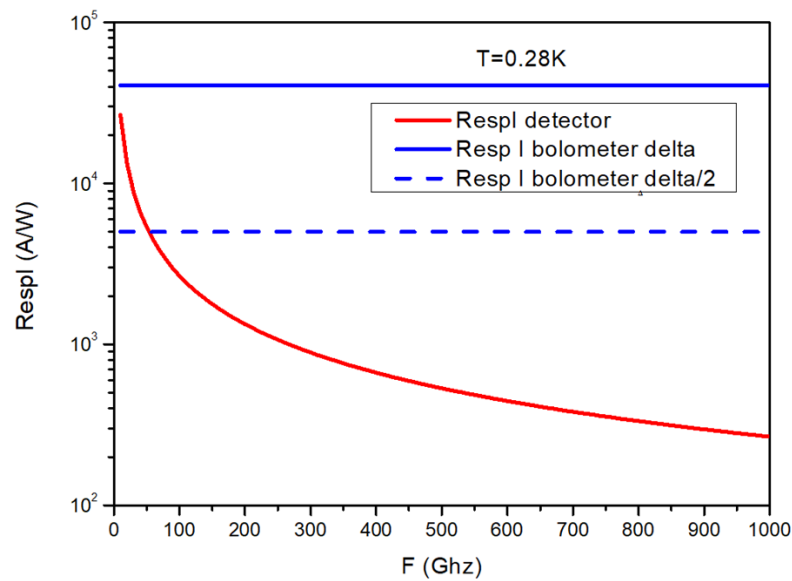


Figure 5. Calculated frequency dependence of current responsivity for the SINIS detector at a bath temperature of 0.28 K. The top blue curve is $\text{Respl} = e/kT$ for a bolometer multiplier at a bias voltage close to the energy gap without strong electron cooling; the dashed blue line is the bias at the half gap with $\text{Respl} = e/2kT$, and the red curve is the photon counter, $\text{Respl} = e/hf$ in the case of strong electron cooling.

Table 1. Current and voltage responsivities for the main SINIS detector operation modes at 350 GHz.

Operation Mode	Current Responsivity	dI/dP (A/W)	dV/dP (V/W)
Photon counter with electron cooling	e/hf	762	2.6×10^7
Practical detector at half gap where $R_d = 35 \text{ k}\Omega$	$2/V_\Delta$	5×10^3	1.75×10^8
Quantum detector close to gap where $R_d = 2 \text{ k}\Omega$	$e/2kT$	2.2×10^4	4.4×10^7
Electric detector at dc	$2k/(R_d e \Sigma \nu T^4)$	3.7×10^5	1.3×10^{10}

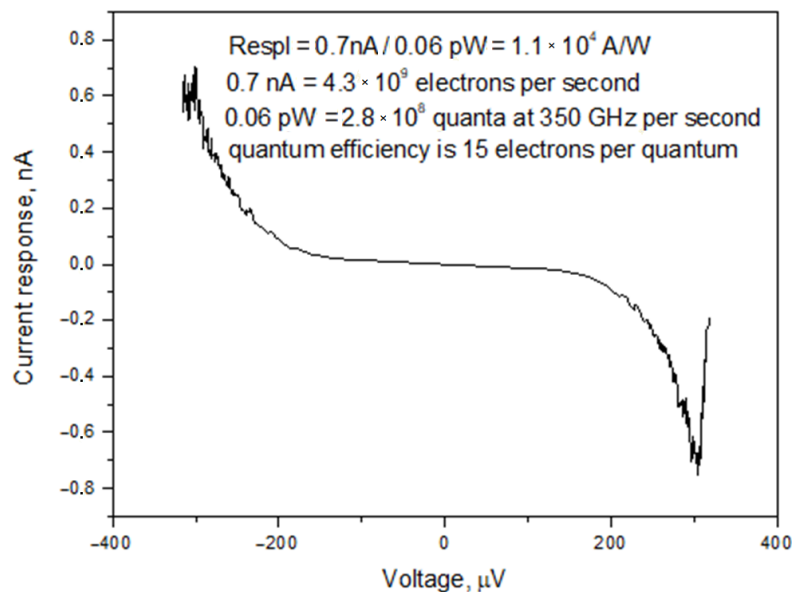


Figure 6. Current response at a bath temperature of 120 mK for a black body radiation power of 60 fW.

4. Traps for Hot Quasiparticles in a Superconductor

The problem of the superconducting electrode overheating as a result of the dc current or background radiation can be rather significant. One of the methods to reduce such overheating is shown in [21], using additional normal metal layers or electrodes. With such a trap, it is possible that the energy of hot quasiparticles will drop down from the gap level to the Fermi level. The question is how to arrange the contact between the S and N electrodes. If direct NS contact is established, the proximity effect can suppress superconductivity, and hot quasiparticles will be reflected from such a boundary due to the effect of Andreev reflection, which will prevent cooling. Tunnel junctions are not affected by either of these effects, but their transparency is rather low compared to that enabled by direct contact. To form a visibly effective NIS trap, its resistance should be very low, and this can be achieved by a very low oxidation dose compared to that of the tunnel barrier of an SINIS bolometer. If the detector resistance is from 1 to 5 k $\Omega/\mu\text{m}^2$, for the NIS trap, it should be from 1 to 10 $\Omega/\mu\text{m}^2$; this is rather problematic, because such junctions suffer from defects and pinholes.

An alternative solution is to significantly increase the superconducting electrodes' volume. We fabricated and measured samples with different volumes of superconducting aluminum and different distances between the NIS junction and normal metal trap [32]. The dynamic resistances of such junctions are presented in Figure 7. The values correspond to the following cases (Figure 7a):

- (1) Superconducting electrodes deposited above the trilayer Ti/Au/Pd normal metal electrodes (distance to the normal metal trap is 2 μm);
- (2) Layout similar to the first, but superconducting electrodes are placed on thin Ti/Pd. In both cases, the ratio of superconducting aluminum to the area of the NIS junction is $S_{Al}/S_{SIN} = 3$;
- (3) The area of the superconducting electrode is much larger, and the superconductor is placed above the normal Ti/Pd, but the distance from the NIS to the normal electrodes is the same as in the previous two;
- (4) The area of superconducting electrodes is increased further ($S_{Al}/S_{SIN} = 200$), and the distance from NIS junctions to normal electrodes is increased to 5 μm .

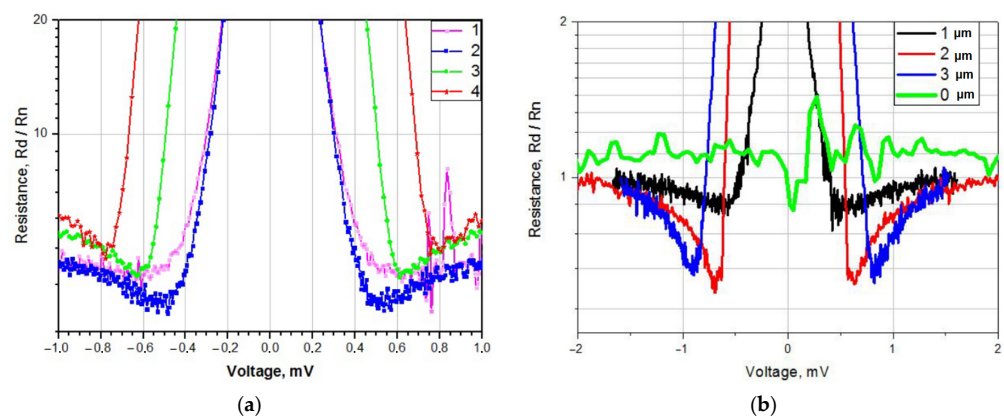


Figure 7. Dynamic resistances of four samples of series connection of two SINIS structures [32]: (a) different volumes of superconducting aluminum (1, 2, 3, and 4 correspond to the description in the text above); (b) different distances between the SIN junction and the normal metal trap.

From Figure 7, we can conclude that the volume of the superconductor and its distance to normal electrodes affect both the energy gap value and the equivalent electron temperature.

5. Fabrication Technology of SINIS

Depending on the available equipment and tasks, different methods of aluminum tunnel junction fabrication can be used. Several technologies are presented in the review paper [33] in detail, and in this paper, we only provide short descriptions and the main principles of such methods. These methods can be divided into two main types: shadow evaporation at tilted angles (Table 2) and direct deposition (Table 3).

Table 2. Comparison of two main shadow technologies for the fabrication of Al tunnel junctions.

Shadow Technique		
Dolan's Bridges	Bridge-Free Technology	
Short description	<ol style="list-style-type: none"> Evaporation of normal metal absorber (Al/Fe) at angle 0° Oxidation of Al layer Evaporation of superconducting Al at angles ± 45° 	<ol style="list-style-type: none"> Evaporation of normal metal absorber (Al/Fe) at angle ± 45° Oxidation of Al layer Rotation of substrate by 90° Evaporation of superconducting Al at angles ± 45°
Schematic image of process	<p>2. Superconductor +45° 1. Absorber 3. Superconductor -45°</p> <p>Insulator, made by oxidation of aluminum</p> <p>Deposition After lift-off</p> <p>1 φ N 2 φ S φ φ</p> <p>N - Normal metal S - Superconductor</p>	
Advantages	Deposition in one vacuum cycle, one lithography	Deposition in one technological process—this technology overcomes the disadvantages of Dolan's suspended bridges
Disadvantages	Possibility of breaking the suspended resist bridge, not completely removing vertical walls, possibly bending the upper layer of the resist; only e-beam lithography; specialized deposition equipment	The common drawback for both shadow evaporation methods is that they require directional evaporation and are not applicable for magnetron sputtering; only e-beam lithography; specialized deposition equipment

Table 3. Comparison of different direct-write technologies for the fabrication of tunnel junctions.

Direct-Write Technology		
Direct-Write Trilayer Technology	Direct-Write Technology	
Short description	<ol style="list-style-type: none"> Deposition of Al layer and oxidation. Then Cu is evaporated as a normal metal electrode of a tunnel junction and covered by Au for passivation Deposition of the normal metal Cu absorber Ar ion-beam etching for removing of Cu and Au from the top of the trilayer structure 	<ol style="list-style-type: none"> Lithography and deposition of the first metal (any type) Lithography, ion etching Deposition of Al and oxidation Deposition of the second metal (any type)
Schematic image of process	<p>Au Cu AlOx Ti</p> <p>AlOx Cu Au Ti</p> <p>Al Cu Au Ti</p> <p>AlOx Cu Au Ti</p> <p>Al Cu Au Ti</p> <p>Si substrate Si substrate Si substrate Si substrate</p> <p>Ar⁺</p> <p>First metal Open window in resist</p> <p>First metal NIS Second metal</p>	

Table 3. Cont.

Direct-Write Technology		
	Direct-Write Trilayer Technology	Direct-Write Technology
Advantages	Any type of lithography	Can be applicable for industrial processes of magnetron sputtering and plasma etching. Such process bring flexibility in the choice of metal film materials and the possibility of creating a high-quality tunnel barrier. Any type of lithography
Disadvantages	Three technological cycles, additional layers for passivation	Two technological cycles

5.1. Shadow Evaporation Technology

Usually, SINIS structures are fabricated by Dolan's technology [34] with suspended bridges of e-beam resist (see Table 2, middle column). Deposition at different angles can be achieved by thermal evaporation using the hot boat, or by e-beam evaporation using a crucible on a tilted holder with a substrate. First, the aluminum layer with an underlayer of Fe is deposited at a normal angle to the substrate. The Fe/Al bilayer is a non-superconducting normal metal due to the suppression of the superconductivity of Al by ferromagnetic Fe. The tunnel barrier is formed via a proper dose of oxygen in the deposition chamber. The top superconducting aluminum layer is deposited at a tilt angle $\pm 45^\circ$. This process can be modified for different angles and thicknesses of both resist layers, which should be exactly calculated. However, the classical Dolan process with a suspended e-beam resist bridge has two basic disadvantages: it is difficult to fabricate the sub-micrometer-size NIS junctions, and it has low reliability due to the sagging and breaking of thin and narrow suspended resist bridges. To solve these problems, bridge-free technology (Table 2, right column) [35,36] was used for the creation of the SINIS structure. Bridge-free technology allows one to fabricate tunnel junctions with areas from $0.01 \mu\text{m}^2$ (and less) to $1000 \mu\text{m}^2$ (and more), improve the size accuracy, increase the reliability and reproducibility, improve the electric conductivity and heat conductivity of the bias wiring via the increase in superconductor thickness, increase the range of exposure dose from 10% to 50%, and increase the possibility of ion cleaning before deposition (there are no thin suspended resist bridges). The key idea of this technology [35,36] is based on the separated deposition of two different metal films into two deep orthogonal grooves in a double-layer resist. The deposition of the first film into the first groove does not lead to deposition in the second groove, because the deposition angle and resist thickness are chosen such that in the deposition into the second groove, the direction is oriented towards the wall of the resist, with subsequent removal together with resist in the lift-off process. Analogously, the second film is deposited into the orthogonal groove when the substrate is rotated by 90° . As a result, only tunnel junctions of the required size remain on the substrate, with the bottom and top electrodes formed along corresponding grooves in the resist. If the sizes of junctions are not large enough, the design can be modified by adding big squares that are slightly shifted towards one another due to the tilt angles and resist thickness.

5.2. Direct Deposition Technology

Shadow evaporation is relatively simple, and allows the depositing of the SINIS structure in one vacuum cycle with one e-beam lithography. However, this method is limited in the dimensions of junctions and in the choice of materials. Besides this, magnetron sputtering is much more widely used, and is the main technology for industrial fabrication. In our earlier work [37], instead of shadow evaporation, we succeeded in fabrication using separate lithography, with a Ti absorber and with magnetron sputtering. The Al technology includes one more step of etching the native aluminum oxide before the fabrication of the tunnel barrier.

All of the technologies that were presented previously have one common feature—the tunnel junction is deposited in one vacuum cycle. This is necessary for the creation of a

high-quality tunnel junction. With separate cycles (lithography of one layer and deposition of the first film, and then a similar procedure for the second), the quality of the tunnel junction will be significantly worse due to the fact that uncontrolled parasitic oxides form on the surface of the first film. To solve this problem, we developed a modified direct-write technology [33,38] (Table 3, right column). The idea is to use ion etching before the deposition of the second layer in the deposition chamber. In this case, the layer of aluminum oxide is removed, and it is possible to oxidize the “clean” aluminum layer, or make an additional thin (a few nm) aluminum layer to be oxidized in order to create a high-quality tunnel barrier. Additionally, such technology allows flexibility in the choice of metal film materials.

Photos of the samples fabricated via different technologies are presented in Figure 8a–d.

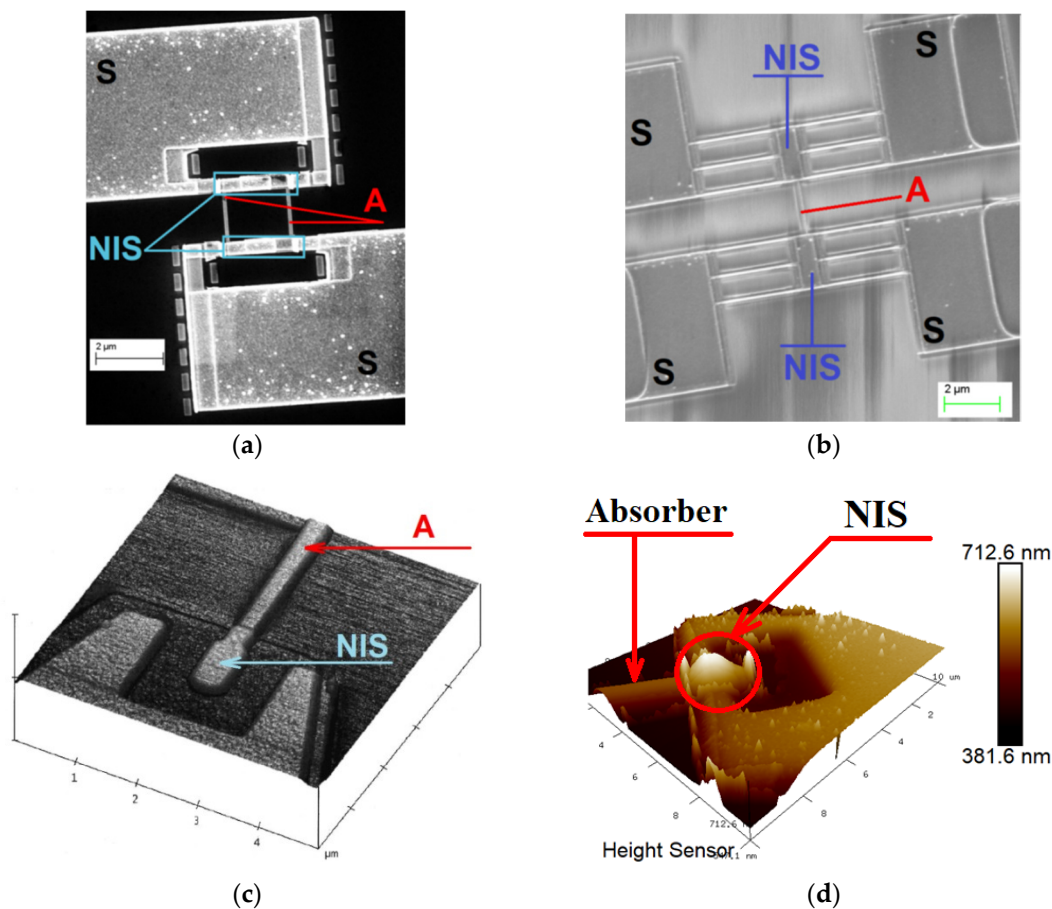


Figure 8. Photos of samples fabricated via different technologies (A—absorber; NIS—normal metal–insulator–superconductor tunnel junction; S—superconducting electrodes): (a) Dolan’s technique; (b) bridge-free technology; (c) direct-write trilayer technology; (d) direct-write separate lithography technology with magnetron sputtering.

5.3. Fabrication of SINIS Junctions with Suspended Absorber

As we mentioned earlier, the need to fabricate SINIS detectors with suspended absorbers is increased by the need to reduce power losses to the substrate and to increase the quantum efficiency of the receiver. The first attempt to realize SINIS structures with suspended absorbers were made in [39,40].

For the creation of such types of SINIS, we used different methods: direct deposition and shadow evaporation. The idea of the direct technology [41] is clear: a trilayer comprising Al–AlO_x–Cu is deposited directly onto the window and then lifted off. In the next step, with laser or e-beam lithography, we open the window in the area where part of the absorber will be suspended. The etching of normal metal Cu in nitric acid around the

superconducting electrodes follows; this additional step allows the improvement of the IV curve, and shows the correct position of the energy gap voltage to be 400 mV. However, this additional step reduces the yield of samples, and it is only possible when using Cu as the absorber. The disadvantage of Cu is that it is rather soft, and it can sag when it is relatively long (a few micrometers). For a schematic image and photo of the SINIS detector with a suspended absorber, see Figure 9.

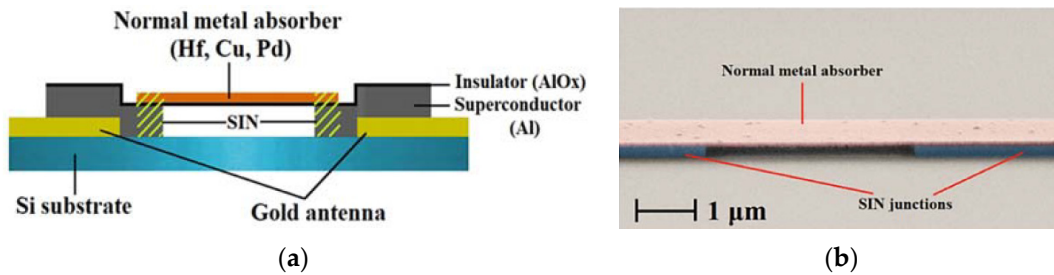


Figure 9. Schematic image (a) and photo (b) of SINIS detector with suspended absorber.

To avoid the chemical etching of a normal metal, we developed a process involving the shadow evaporation of the normal metal in the required area. A schematic view of this fabrication process is presented in Figure 10. This technology requires rather thick resists of over 900 nm. The absorber film is only deposited in the wider area, and in narrow (about 1 μm wide) areas, the metal is evaporated onto the wall of the resistor, before finally being removed together with the resist in the lift-off step. The process of Al with bridge etching is the same as in the previous process using Cu. SEM views of such samples are presented in Figure 11.

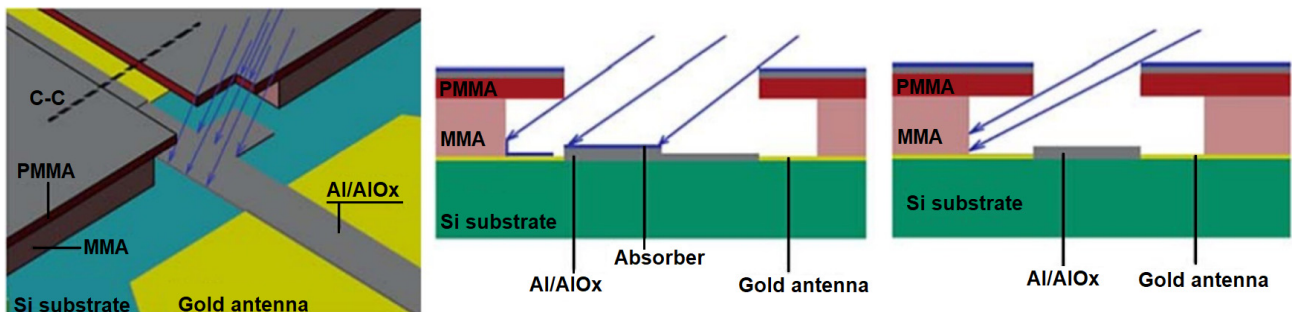


Figure 10. Schematic view of the process with the shadow evaporation of the normal metal in the required area [33].

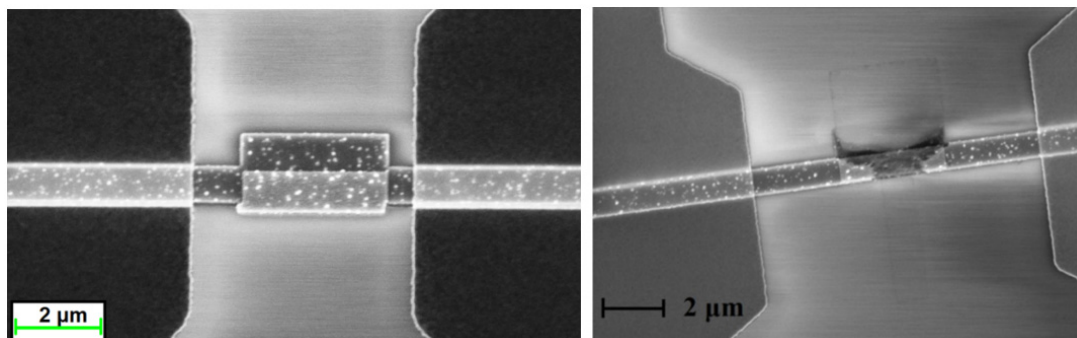


Figure 11. SEM images with examples of SINIS detectors with a suspended Hafnium absorber before (left) and after (right) aluminum etching under the absorber [33].

6. Experimental Studies

The fabricated samples were measured in two cryostats: the Heliox AC-V from Oxford Instruments (Abingdon, Oxfordshire, England) with an operation temperature as low as 273 mK, and a cryostat insert designed by V. Edelman at the Kapitza Institute for Physical Problems (Moscow, Russia) [42], with an operation temperature as low as 50 mK.

Sensitive experiments were performed in the dilution cryostat, which was inserted into the transport He dewar [42]. The lowest achieved temperature was 50 mK. Such a cryostat does not require external pumps that significantly reduce vibrations and electric jamming. By using a cryostat equipped with three sample holders, in one cooling cycle, it is possible to measure and compare the characteristics of three samples. The cryostat was equipped with a blackbody radiation source, and we studied the responsivity and dynamic range of samples at different radiation temperatures (the schematic of this experiment is presented in Figure 12) [14].

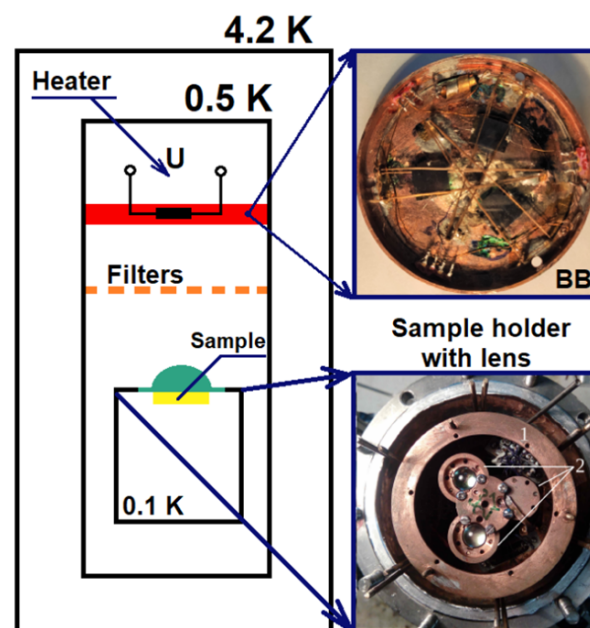


Figure 12. Schematic view of experimental setup (left). Photos from [43], **top**—He3 radiation shield with blackbody source; **bottom**—sample holders with sapphire lenses.

The optical response of the SINIS detectors with integrated twin-slot antennas, designed for the 350 GHz band, was measured at a phonon temperature around 100 mK using a blackbody radiation source [14]. Three blackbody sources were placed on the top covers of the sample chambers to illuminate each sample separately. A thin film of NiCr on a sapphire or silicon substrate, with contact pads for the heating current and a thermometer for temperature control, was used as such a blackbody radiation source. Mesh bandpass filters were used to determine the actual bandwidth of the incoming signal and suppress the background radiation. A diaphragm and bandpass filter between the BB source and the SINIS detector were used to suppress out-of-band background radiation.

A current response of 0.7 nA in the SINIS with a suspended Cu absorber at a radiation power of 0.06 pW corresponds to a current responsivity of 1.1×10^4 A/W. The detected current of 0.7 nA corresponds to 4.3×10^9 electrons per second, and a power of 0.06 pW corresponds to 2.8×10^8 photons at 350 GHz per second. The quantum efficiency in this case was over 15 electrons per absorbed radiation photon [14].

7. Applications of SINIS Detectors

Sub-terahertz detectors are intended for applications in various fields of science [44–46], astronomy [47,48], technology, commercial applications, telecommunications [49–51], mili-

tary applications [52–54], security systems, and life sciences. Astronomy sets the highest requirements for detector sensitivity and wide dynamic range, as primarily this is fundamentally important for ground-based observatories. In telecommunications, there is an urgent need to improve the performance of telecommunications channels, which can be solved by moving from the current satellite communications and mobile communications from centimeter waves to shorter waves. The growing demand for high-speed wireless channels has indicated a trend towards an increase in the signal frequencies towards 24–100 GHz for 5G, 140 GHz, 220 GHz, and 340 GHz for 6G, and 700 GHz suggested for 7G [55]. The optical range is poorly suited for creating cellular data transmission networks due to the suppression of transmission in rain, snow, and fog. Moreover, sub-THz telecommunications can be used to create secure communications for military applications. In radar systems, two areas can be distinguished: military applications (aircraft detection and the detection of anti-personnel mines), and a relatively new “problem”—the detection of space threats (such as asteroid–comet hazards, space debris, and space weather).

8. Discussion

The key features of SINIS detectors and the achieved performance are closely related to the proper modeling microwave absorption, power losses, and the electron and phonon cooling balance. In a recent publication [56], the authors estimated the voltage responsivity as $dV/dP = 2k/(e\Sigma\nu T_e^4)$, which brings 2.5×10^{10} V/W at $T_e = 100$ mK, 1.5×10^9 V/W at $T_e = 200$ mK and 3×10^8 V/W at $T_e = 300$ mK. According to their experimental curves, the voltage responsivity is 1.5×10^9 V/W at a phonon temperature of 200 mK, an electron temperature of 120 mK, and a 0.3 pW absorbed power. This means that electron cooling does not improve sensitivity. For an estimated electron temperature of 130 mK, the responsivity (according to a simple estimation from the electron temperature alone) should be over 10^{10} V/W. In [56], the NEP = 3×10^{-17} W/Hz^{1/2} at a bath temperature of 200 mK and NEP = 6×10^{-17} W/Hz^{1/2} at a bath temperature of 200 mK for $T_e = 120$ mK and 200 mK. The overestimated readout amplifier noise 20 nV/Hz^{1/2} should bring a corresponding NEP = 2×10^{-18} and 6×10^{-18} W/Hz^{1/2}. One order of magnitude difference means that electron cooling does not result in the expected improvement, which confirms our model of a quantum detector.

The main differences from earlier studies, and the novel insights we offer, are as follows: using a quantum absorption model instead of simple bolometric response; there was no significant improvement caused by direct electron cooling in the same SINIS; using a suspended absorber instead of an absorber on the substrate; and increasing the volume of the superconductor instead of direct N traps for the cooling of superconducting electrodes. Our future research will be oriented towards SINIS samples with suspended heavy normal metal absorbers and thick superconducting antennas and wiring.

9. Conclusions

Over the last 30 years, a wide family of quantum SINIS detectors has been designed, fabricated, and experimentally studied at frequencies up to terahertz [57] and bath temperatures down to 50 mK. At 350 GHz, such detectors demonstrate a current responsivity of 10^4 A/W and a temperature responsivity down to 1.6 μ K/Hz^{1/2}, while detectors with a suspended absorber demonstrate a quantum efficiency of 15 electrons per photon. A novel fabrication technology was developed to enact the transfer from shadow evaporation to magnetron sputtering with separate electron lithography.

10. Patents

1. Tarasov, M.; Nagirnaya, D.; Gunbina, A.; Fominsky, M.; Yusupov, R. Metal-Dielectric-Metal-Dielectric-Metal photodetector, Patent RU2749575C1, Russia, date of publication: 15 June 2021, priority: 7 September 2020.

2. Tarasov, M.; Gunbina, A.; Nagirnaya, D.; Fominskii, M. Method of Making Device with Thin-Film Tunnel Junctions, Patent RU2733330C1, date of publication: 1 October 2020, priority: 22 July 2019.
3. Tarasov, M.; Gunbina, A.; Fominsky, M.; Chekushkin, A.; Method of fabrication of thin-film tunnel junctions by means of separate lithography, application for patent, Patent RU2757762C1, date of publication: 21 October 2021, priority: 30 March 2021.
4. Tarasov, M.; Chekushkin, A.; Yusupov, R. Method of fabrication devices with free-standing microbridges, Patent RU2632630C1, date of publication: 6 October 2017, priority: 6 June 2016.

Author Contributions: Conceptualization, M.T. and V.E.; methodology, M.T.; software, R.Y.; validation, A.G., A.C., and R.Y.; resources, V.K.; data curation, R.Y.; writing—original draft preparation, A.G.; writing—review and editing, V.K.; visualization, A.G.; supervision, M.T.; project administration, V.K.; funding acquisition, V.K. All authors have read and agreed to the published version of the manuscript.

Funding: This work was supported by a grant from the Russian Foundation for Basic Research project No. 19-52-80023; tunnel structures were made in V. Kotelnikov IRE RAS within the framework of the state assignment. The equipment of USU “Cryointegral” was used to carry out the research; USU is supported by a grant from the Ministry of Science and Higher Education of the Russian Federation, agreement No. 075-15-2021-667.

Institutional Review Board Statement: Not applicable.

Informed Consent Statement: Not applicable.

Acknowledgments: The authors acknowledge M. Fominsky for e-beam lithography and SEM analysis, S. Kraevsky for AFM analysis, and S. Lemzyakov for help in experiments.

Conflicts of Interest: The authors declare no conflict of interest.

References

1. Giazotto, F.; Heikkilä, T.T.; Luukanen, A. Electronic Refrigeration: Physics and Applications. Available online: <https://arxiv.org/pdf/cond-mat/0508093v1.pdf> (accessed on 19 September 2022).
2. Ullom, J.N. Physics and applications of NIS junctions. *Proc. AIP Conf.* **2002**, *605*, 135–140. [\[CrossRef\]](#)
3. Tarasov, M.; Edelman, V. Nanodevices with Normal Metal—Insulator—Superconductor Tunnel Junctions. In *Functional Nanostructures and Metamaterials for Superconducting Spintronics: From Superconducting Qubits to Self-Organized Nanostructures*; Sidorenko, A., Ed.; Springer International Publishing AG: Cham, Switzerland, 2018; pp. 91–116. [\[CrossRef\]](#)
4. Vystavkin, A.; Shuvaev, D.; Kuz'min, L.; Tarasov, M.A.; Aderstedt, E.; Claeson, M.W.T. Normal-metal hot-electron bolometer with Andreev reflection from superconductor boundaries. *J. Exp. Theor. Phys.* **1999**, *88*, 598–602. [\[CrossRef\]](#)
5. Nahum, M.; Richards, P.; Mears, C. Design analysis of a novel hot-electron microbolometer. *IEEE Trans. Appl. Supercond.* **1993**, *3*, 2124–2127. [\[CrossRef\]](#)
6. Chouvaev, D.; Sandgren, D.; Tarasov, M.; Kuzmin, L. Optical Qualification of the Normal Metal Hot-Electron Microbolometer (NHEB). In Proceedings of the 12th International Symposium on Space Terahertz Technology, San Diego, CA, USA, 14–16 February 2001.
7. Kuzmin, L.S. Cold-Electron bolometers. In *Bolometers*; Perera, A.G.U., Ed.; InTech: Rijeka, Croatia, 2012; p. 77. ISBN 978-953-51-0235-9.
8. Brien, T.L.R.; Ade, P.A.R.; Barry, P.S.; Dunscombe, C.; Leadley, D.R.; Morozov, D.V.; Myronov, M.; Parker, E.H.; Prest, M.J.; Prunnila, M.; et al. A strained silicon cold electron bolometer using Schottky contacts. *Appl. Phys. Lett.* **2014**, *105*, 043509. [\[CrossRef\]](#)
9. Schmidt, D.R.; Duncan, W.D.; Irwin, K.D.; Lehnert, K.W.; Miller, N.A.; Ullom, J.N. Normal metal–insulator–superconductor junction technology for bolometers. *Nucl. Instrum. Methods Phys. Res. Sect. A Accel. Spectrom. Detect. Assoc. Equip.* **2006**, *559*, 516–518. [\[CrossRef\]](#)
10. Schmidt, D.R.; Lehnert, K.W.; Clark, A.M.; Duncan, W.D.; Irwin, K.D.; Miller, N.; Ullom, J.N. A superconductor–insulator–normal metal bolometer with microwave readout suitable for large-format arrays. *Appl. Phys. Lett.* **2005**, *86*, 053505. [\[CrossRef\]](#)
11. Tarasov, M.; Gunbina, A.; Mansfeld, M.; Yakopov, G.; Chekushkin, A.; Yusupov, R.; Lemzyakov, S.; Edelman, V.; Vdovin, V. Arrays of annular cryogenic antennas with SINIS bolometers and cryogenic receivers for SubTHz observatories. *EPJ Web Conf.* **2018**, *195*, 05010. [\[CrossRef\]](#)
12. Devyatov, I.A.; Krutitskii, P.A.; Kupriyanov, M.Y. Investigation of various operation modes of a miniature superconducting detector of microwave radiation. *JETP Lett.* **2006**, *84*, 57–61. [\[CrossRef\]](#)

13. Devyatov, I.A.; Kupriyanov, M.Y. Investigation of a nonequilibrium electron subsystem in low-temperature microwave detectors. *JETP Lett.* **2004**, *80*, 646–650. [[CrossRef](#)]
14. Yusupov, R.A.; Gunbina, A.A.; Chekushkin, A.M.; Nagirnaya, D.V.; Lemzyakov, S.A.; Edel'man, V.S.; Tarasov, M.A. Quantum response of a bolometer based on the SINIS structure with a suspended absorber. *Phys. Solid State* **2020**, *62*, 1567–1570. [[CrossRef](#)]
15. Feshchenko, A.V.; Casparis, L.; Khaymovich, I.M.; Maradan, D.; Saira, O.P.; Palma, M.; Meschke, M.; Pekola, J.P.; Zumbühl, D.M. Tunnel-Junction Thermometry Down to Millikelvin Temperatures. *Phys. Rev. Appl.* **2015**, *4*, 034001. [[CrossRef](#)]
16. Pekola, J. Trends in Thermometry. *J. Low Temp. Phys.* **2004**, *135*, 723–744. [[CrossRef](#)]
17. Isoaari, E.; Holmqvist, T.; Meschke, M.; Heinonen, M.; Pekola, J.P. Thermometry by micro and nanodevices. *Eur. Phys. J. Spec. Top.* **2009**, *172*, 323–332. [[CrossRef](#)]
18. Pekola, J.P.; Manninen, A.J.; Leivo, M.M.; Arutyunov, K.; Suoknuuti, J.K.; Suppala, T.I.; Collaudin, B. Microrefrigeration by quasiparticle tunneling in NIS and SIS junctions. *Phys. B Condens. Matter* **2000**, *280*, 485–490. [[CrossRef](#)]
19. Nguyen, H.Q.; Aref, T.; Kauppila, V.J.; Meschke, M.; Winkelmann, C.B.; Courtois, H.; Pekola, J.P. Trapping hot quasi-particles in a high-power superconducting electronic cooler. *New J. Phys.* **2013**, *5*, 085013. [[CrossRef](#)]
20. Clark, A.M.; Miller, N.A. Cooling of bulk material by electron-tunneling refrigerators. *Appl. Phys. Lett.* **2005**, *86*, 173508. [[CrossRef](#)]
21. O'Neil, G.C. Improving NIS Tunnel Junction Refrigerators: Modeling, Materials, and Traps. Ph.D. Thesis, University of Colorado, Boulder, CO, USA, 2011.
22. Kuzmin, L.; Fominsky, M.; Kalabukhov, A.; Golubev, D.; Tarasov, M. Capacitively Coupled Hot-Electron Nanobolometer with SIN Tunnel Junctions. In Proceedings of the SPIE Volume 4855: Millimeter and Submillimeter Detectors for Astronomy, Astronomical Telescopes and Instrumentation, Waikoloa, HI, USA, 17 February 2003. [[CrossRef](#)]
23. Tarasov, M.; Nagirnaya, D.; Gunbina, A.; Fominsky, M.; Yusupov, R. Metal-Dielectric-Metal-Dielectric-Metal Photodetector. Patent RU2749575C1, 15 June 2021.
24. Tarasov, M.; Edelman, V.; Lemzyakov, S.; Gunbina, A.A.; Yusupov, R.A.; Chekushkin, A.M.; Nagirnaya, D.V.; Vdovin, V.F.; Kalaboukhov, A. Cryogenic Mimim and Simis Microwave Detectors. In Proceedings of the 7th All-Russian Microwave Conference (RMC), Moscow, Russia, 25–27 November 2020; pp. 25–27. [[CrossRef](#)]
25. Tarasov, M.; Fominsky, M.; Kalabukhov, A.; Kuzmin, L. Experimental study of a bolometer on hot electrons in normal metal with capacitive coupling. *JETP Lett.* **2002**, *76*, 507–510. [[CrossRef](#)]
26. Nahum, M.; Eiles, T.M.; Martinis, J.M. Electronic microrefrigerator based on a normal-insulator-superconductor tunnel junction. *Appl. Phys. Lett.* **1994**, *65*, 3123–3125. [[CrossRef](#)]
27. Leivo, M.M.; Pekola, J.P.; Averin, D.V. Efficient Peltier refrigeration by a pair of normal metal/insulator/superconductor junctions. *Appl. Phys. Lett.* **1996**, *68*, 1996–1998. [[CrossRef](#)]
28. Kuzmin, L.S.; Devyatov, I.A.; Golubev, D. Cold-electron bolometer with electronic microrefrigeration and general noise analysis. In Proceedings of the Millimeter and Submillimeter Waves IV Volume 3465, SPIE's International Symposium on Optical Science, Engineering, and Instrumentation, San Diego, CA, USA, 13 November 1998; pp. 193–199.
29. Golubev, D.; Kuzmin, L. Nonequilibrium theory of a hot-electron bolometer with normal metal-insulator-superconductor tunnel junction. *J. Appl. Phys.* **2001**, *89*, 6464. [[CrossRef](#)]
30. Gunbina, A.; Lemzyakov, S.; Tarasov, M.; Edelman, V.S.; Yusupov, R.A.B. Response of a SINIS detector with electron cooling to submillimeter-wave radiation. *JETP Lett.* **2020**, *11*, 539–542. [[CrossRef](#)]
31. Tarasov, M.; Gunbina, A.; Yusupov, R.; Chekushkin, A.; Nagirnaya, D.; Lemzyakov, S.; Vdovin, V.; Edelman, V.; Kalaboukhov, A.; Winkler, D. Thermal absorption and quantum efficiency of SINIS bolometer. *IEEE Trans. Appl. Supercond.* **2021**, *31*, 2300105. [[CrossRef](#)]
32. Chekushkin, A.; Tarasov, M.; Yusupov, R.; Edelman, V. Influence of normal metal traps, Andreev reflection and proximity effect on superconductor cooling in SINIS-structures. *Work. MIPT* **2018**, *10*, 64–71.
33. Gunbina, A.; Tarasov, M.; Fominsky, M.; Chekushkin, A.; Yusupov, R.; Nagirnaya, D. Fabrication of Aluminium Nanostructures for Microwave Detectors Based on Tunnel Junctions. In *Advances in Microelectronics Reviews*; Yurish, S.Y., Ed.; IFSA Publishing, S.L.: Barcelona, Spain, 2021; Volume 3, pp. 183–212.
34. Dolan, G.J. Offset mask for lift-off photoprocessing. *Appl. Phys. Lett.* **1977**, *31*, 337–339. [[CrossRef](#)]
35. Lecocq, F.; Pop, I.M.; Peng, Z.; Matei, I.; Crozes, T.; Fournier, T.; Naud, C.; Guichard, W.; Buisson, O. Junction fabrication by shadow evaporation without a suspended bridge. *Nanotechnology* **2011**, *22*, 315302. [[CrossRef](#)] [[PubMed](#)]
36. Tarasov, M.; Gunbina, A.; Nagirnaya, D.; Fominsky, M. Method of Making Device with Thin-Film Tunnel Junctions. Patent RU2733330C1, 1 October 2020.
37. Otto, E.; Tarasov, M.; Grimes, P.; Chekushkin, A.; Kuzmin, L.S.; Yassin, G. Optical response of a titanium-based cold-electron bolometer. *Supercond. Sci. Technol.* **2013**, *26*, 085020. [[CrossRef](#)]
38. Tarasov, M.; Gunbina, A.; Fominsky, M.; Chekushkin, A. Method of Fabrication of Thin-Film Tunnel Junctions by Means of Separate Lithography, Application for Patent. Patent RU2757762C1, 21 October 2021.
39. Tarasov, M.; Edelman, V.; Mahashabde, S.; Fominsky, M.; Lemzyakov, S.; Chekushkin, A.; Yusupov, R.; Winkler, D.; Yurgens, A. Electrical and optical properties of a bolometer with a suspended absorber and tunneling-current thermometers. *Appl. Phys. Lett.* **2017**, *110*, 242601. [[CrossRef](#)]
40. Tarasov, M.; Edelman, V.; Mahashabde, S.; Fominsky, M.; Lemzyakov, S.; Chekushkin, A.; Yusupov, R.; Winkler, D.; Yurgens, A. SINIS bolometer with a suspended absorber. *J. Phys. Conf. Ser.* **2017**, *969*, 012088. [[CrossRef](#)]

41. Tarasov, M.; Chekushkin, A.; Yusupov, R. Method of Fabrication Devices with Free-Standing Microbridges. Patent RU2632630C1, 6 October 2017.
42. Edelman, V.S. A dilution microcryostat-insert. *Instrum. Exp. Tech.* **2009**, *52*, 301–307. [[CrossRef](#)]
43. Lemzyakov, S. Interaction of SINIS Structures with Submillimeter-Wave Radiation. Ph.D. Thesis, P. Kapitza Institute for Physical Problems, Moscow, Russia, 2020.
44. Pfeiffer, U. Integrated Circuit Design for Terahertz Applications. 6G Wireless Summit. 2019; 201p.
45. Lu, X.; Venkatesh, S.; Saeidi, H. A Review on Applications of Integrated Terahertz Systems. *China Commun.* **2021**, *18*, 175–201. [[CrossRef](#)]
46. Pavlidis, D. *Fundamentals of Terahertz Devices and Applications*; John Wiley & Sons: Hoboken, NJ, USA, 2021; 576p, ISBN 1119460735.
47. Beckman, J.E. Radioastronomy. In *Multimessenger Astronomy*; Springer International Publishing AG: Cham, Switzerland, 2021; pp. 45–79. [[CrossRef](#)]
48. Hojaev, A.S.; Zinchenko, I.I. Scientific Problems and Possibilities of Studying Extended Molecular Clouds with RT-70. *Bull. Lebedev Phys. Inst.* **2021**, *48*, 272–280. [[CrossRef](#)]
49. Editors: Ghzaoui, M.E.; Das, S.; Lenka, T.R.; Biswas, A. *Terahertz Wireless Communication Components and System Technologies*; Springer International Publishing AG: Cham, Switzerland, 2022; ISBN 978-981-16-9181-2.
50. Chaccour, C.; Soorki, M.N.; Saad, W.; Bennis, M.; Popovski, P.; Debbah, M. Seven Defining Features of Terahertz (THz) Wireless Systems: A Fellowship of Communication and Sensing. *IEEE Commun. Surv. Tutor.* **2022**, *24*, 967–993. [[CrossRef](#)]
51. Akyildiz, I.F.; Han, C.; Hu, Z.; Nie, S.; Jornet, J.M. Terahertz Band Communication: An Old Problem Revisited and Research Directions for the Next Decade. *IEEE Trans. Commun.* **2022**, *70*, 4250–4285. [[CrossRef](#)]
52. Meenakshi; Saurav, P.; Kishor, K. Design and simulation of metamaterial under the THz frequency for short-range wireless communication and military purposes. *Mater. Today Proc.* **2022**, *62*, 3729–3733. [[CrossRef](#)]
53. Ergün, S.; Sönmez, S. Terahertz Technology for Military Applications. *J. Manag. Inf. Sci.* **2015**, *3*, 13–16. [[CrossRef](#)]
54. Dodson, C.; Fitch, M.J.; Osiander, R.; Spicer, J.B. Terahertz imaging for anti-personnel mine detection. *Proc. Terahertz Mil. Sec. Appl. III* **2005**, *5790*, 85–93. [[CrossRef](#)]
55. Rappaport, T.S.; Xing, Y.; Kanhere, O.; Ju, S. Wireless Communications and Applications Above 100 GHz: Opportunities and Challenges for 6G and Beyond. *IEEE Access.* **2019**, *7*, 78729–78757. [[CrossRef](#)]
56. Kuzmin, L.S.; Pankratov, A.L.; Gordeeva, A.V.; Zbrozhek, V.O.; Shamporov, V.A.; Revin, L.S.; Blagodatkin, A.V.; Masi, S.; de Bernardis, P. Photon-noise-limited cold-electron bolometer based on strong electron self-cooling for high-performance cosmology missions. *Commun. Phys.* **2019**, *2*, 104. [[CrossRef](#)]
57. Tarasov, M.; Kuzmin, L.; Stepantsov, E.; Agulo, I.; Kalabukhov, A.; Fominskii, M.; Ivanov, Z.; Claeson, T. Terahertz spectroscopy by Josephson oscillator and SINIS bolometer. *JETP Lett.* **2004**, *79*, 298–303. [[CrossRef](#)]